

Oxygen and dioxygen centers in Si and Ge: Density-functional calculations

J. Coutinho and R. Jones

School of Physics, The University of Exeter, Exeter EX4 4QL, United Kingdom

P. R. Briddon

Department of Physics, The University of Newcastle upon Tyne, Newcastle upon Tyne NE1 7RU, United Kingdom

S. Öberg

Department of Mathematics, University of Luleå, Luleå S-97187, Sweden

(Received 20 May 2000)

Ab initio density-functional calculations using Gaussian orbitals are carried out on large Si and Ge supercells containing oxygen defects. The formation energies, local vibrational modes, and diffusion or reorientation energies of O_i , O_{2i} , VO, VOH, and VO_2 are investigated. The piezospectroscopic tensors for O_i , VO, and VO_2 are also evaluated. The vibrational modes of O_i in Si are consistent with the view that the defect has effective D_{3d} symmetry at low hydrostatic pressures but adopts a buckled structure for large pressures. The anomalous temperature dependence of the modes of O_{2i} is attributed to an increased buckling of Si-O-Si when the lattice contracts. The diffusion energy of the dimer is around 0.8 eV lower than that of O_i in Si and 0.6 eV in Ge. The dimer is stable against VO or VO_2 formation and the latter defect has modes close to the reported 894-cm^{-1} band. The reorientation energies for O and H in VO and VOH defects are found to be a few tenths of an eV and are greater when the defect has trapped an electron.

I. INTRODUCTION

Oxygen is the most common and best studied impurity in Si produced by the Czochralski (Cz) method and recent reviews are found in Refs. 1–3. Nevertheless, in spite of work extending over 50 years, many of its properties remain poorly understood. Even the structure of the isolated interstitial impurity—long believed to be a simple bent Si-O-Si unit similar to the arrangement in quartz—has come under recent debate. Detailed analysis of its far infrared local vibrational modes (LVM's) has suggested that the energy barrier between the bent form with an Si-O-Si angle of around 160° , and the highly symmetrical configuration where the O atom lies at the bond center (BC) is negligible. Thus the O atom tunnels between equivalent sites around the bond center, effectively assuming D_{3d} symmetry with an Si-O-Si angle of 180° .

Another dramatic suggestion is that the aggregation of two O atoms leading to an oxygen dimer does not lead to the ejection of a Si interstitial forming a VO_2 center, but is a defect with the remarkable property of migrating through the lattice at a rate faster than that of the single interstitial. This result has led to a reappraisal of both the rates at which larger oxygen clusters form, and the oxygen composition of the thermal donor defects which arise after sustained annealing of Cz Si below about 450°C .⁴

We report here details of the structure, energetics, and vibrational behavior of a number of oxygen defects in Si and Ge. We use a supercell code that incorporates the localized basis function of the Cartesian Gaussian type. The great advantage of supercell methods over clusters is that energy convergence is easier to obtain and that these energies are unaffected by the location of the defect within the supercell.

In a cluster, the energies of defects can be sensitive to their location.

In Sec. II we describe details of the technique and discuss convergence issues. In Sec. III we apply the formalism to a single oxygen atom in a supercell. We find that in Si the ground state has a buckled form with C_2 symmetry with a Si-O-Si angle of 158° and the barrier of only 13 meV to the D_{3d} form where the angle is 180° . This energy is within the error in the calculations and thus the results are consistent with the modern view that the oxygen atom is delocalized. However, the tunneling model cannot account for the effect of pressure on the asymmetric stretch mode at 1136 cm^{-1} .⁵ We show that if the defect maintained D_{3d} symmetry then this frequency increases with pressure. In contrast, the frequency of the corresponding mode in the C_2 defect decreases with pressure, in agreement with experiment, and this is simply understood in terms of an increased buckling under stress. Our view then is that the structure of this defect in Si is highly sensitive to external conditions and is different for high pressures. We also extend the calculations to Ge where there is much less information available on oxygen defects.

An important characteristic of an anisotropic defect is the stress or piezospectroscopic tensor.⁶ In the absence of any imposed stress, isolated point defects are equally distributed over all orientations related by the symmetry of the lattice. Thus O_i inhabits with equal probabilities the four possible $\langle 111 \rangle$ alignments. Inserting oxygen into Si with random alignment causes a volume increase but no shape change. However, imposing a stress across, say, a particular (111) face results in an energy increase of those oxygen atoms with this alignment, and a decrease in the energy of those with different alignments. The increase in energy is written $\Delta E_i = \text{Tr} A_i \sigma$ where σ is the imposed stress tensor and A_i is the strain-energy tensor for the oxygen atom with alignment i .

The stress and strain tensors, σ and ϵ , are related by the elastic constants of the material and the energy can be written as $\Delta E_i = \text{Tr} B_i \epsilon$ where B is the traceless stress-energy tensor. At a temperature where the oxygen atoms are mobile, then the equilibrium population of oxygen atoms with alignment i is related to ΔE_i and can be measured by spectroscopic techniques. We evaluate this quantity for both substitutional and interstitial oxygen and their disparity provides further evidence for the state of oxygen in Si.

The diffusion of interstitial oxygen is considered in Sec. IV. Detailed experimental studies have established that the process is governed by the hopping of a single oxygen atom between bond-centered sites with an activation energy of 2.53 eV.⁷ However, theoretical studies have enjoyed mixed success in reproducing this fundamental property. An early cluster calculation gave 2.8 eV but this value has not been found by supercell calculations.⁸⁻¹¹ The diffusion barrier is the energy difference between the buckled stable configuration and the saddle point which has long been considered to be the Y -lid configuration where the oxygen atom lies midway between two second-neighboring Si atoms. This energy difference has been found to be about 1.8–2.2 eV and it has been suggested that this discrepancy arises from the neglect of the kinetic energy of the O atom,¹² and subsequently to the neglect of a simultaneous motion of Si neighbors.⁸ However, reaction rate theory includes both of these effects and assumes only that an oxygen atom once reaching the saddle point executes a diffusive step.¹³ We find that the activation energy is weakly sensitive to the size of the cell and becomes 2.2 eV for cells that range from 64 to 128 silicon atoms.

In Sec. V we turn to oxygen dimers. Previous work on the binding energy of oxygen atoms within the dimer in Si gave values between 0.2 and 1.0 eV compared with the experimental value of 0.3 eV.¹⁴ Recently, it was found that there were two structures of the dimer with competitive energies.¹⁵ These consisted of a pair of oxygen atoms at neighboring BC sites sharing a common Si atom (staggered dimer), and a pair lying on the hexagonal ring but separated by a Si-Si bond (skewed dimer). Our earlier work suggested that the skewed dimer possessed LVM's in better agreement with experiment. However, the contrary conclusion was reached by Pesola *et al.*¹⁶ A fresh look at this problem has concluded that Pesola *et al.* are correct and the observed modes correspond with those of the staggered dimer. A characteristic feature of the dimer frequencies is that they shift downwards with temperature. This is unusual as the accompanying lattice contraction compresses bonds and this is expected to lead to an increase in their frequencies. However, the anomalous effect can be explained as an increased buckling in the same way that pressure affects the modes of the isolated interstitial oxygen center. This suggests that whenever interstitial oxygen atoms in Si are squeezed out of the bond centers as in a buckled configuration, the fundamental stretch mode may possess a weak or anomalous temperature dependence.

We also demonstrate that dimer formation is energetically favorable over the formation of a vacancy-dioxygen (VO_2) defect. In common with earlier results^{17,18} we show that the dimer in Si moves with a modest migration energy of about 1.4 eV and such an effect may explain why oxygen aggregates containing many oxygen atoms can rapidly arise during anneals at temperatures where dimers are stable.

Finally, the interaction of a single hydrogen atom with VO is discussed and especially the reorientation energies of O and H in the neutral and negatively charged state. These energies turn out to be a few tenths of an eV although the defect itself is stable to high temperatures around 300 °C. Many of these investigations are repeated for oxygen defects in Ge where there is less experimental knowledge and the results here should serve as a challenge to experimentalists.

II. METHOD

The calculations used local density-functional theory with a Perdew-Wang exchange-correlation energy parametrization¹⁹ together with Bachelet-Hamann-Schlüter (BHS) pseudopotentials.²⁰ The basis consisted of Cartesian Bloch-Gaussian orbitals $B_{i,\mathbf{k}}(\mathbf{r})$ which involve a sum of Gaussian orbitals ϕ_i over lattice vectors \mathbf{R}_L ,

$$B_{i,\mathbf{k}}(\mathbf{r}) = \frac{1}{\sqrt{N}} \sum_L e^{i\mathbf{k} \cdot \mathbf{R}_L} \phi_i(\mathbf{r} - \mathbf{R}_i - \mathbf{R}_L).$$

These basis functions are located at both nuclei and bond center sites \mathbf{R}_i within the unit cell. If the coefficients of these basis functions in the m, \mathbf{k} state is $c_i(m, \mathbf{k})$ then the charge density can be written as

$$n(\mathbf{r}) = \sum_{ij\mathbf{k}} b_{ij,\mathbf{k}} B_{i,\mathbf{k}}^*(\mathbf{r}) B_{j,\mathbf{k}}(\mathbf{r}),$$

$$b_{ij,\mathbf{k}} = \sum_m f_{m,\mathbf{k}} c_i^*(m, \mathbf{k}) c_j(m, \mathbf{k}).$$

Here $f_{m,\mathbf{k}}$ is the occupancy of the m, \mathbf{k} state. Matrix elements of the kinetic energy and the pseudopotentials are found in real space while the Hartree and exchange-correlation energies and potentials are found from a Fourier expansion of the charge density and exchange-correlation terms, respectively. The calculations are self-consistent and analytic expressions for the forces acting on atoms are found from the Hellmann-Feynman theorem but include a Pulay term coming from the dependence of the basis set on the nuclear sites. All atoms in the supercell were relaxed or subject to a specific constraint, until the maximum force on an atom is less than 0.03 eV/Å. An advantage of the Gaussian basis sets used to describe the wave functions over a plane-wave basis is that one can converge the formation energy of a defect in a Si supercell with 22 orbitals per atom as opposed to about 100 plane waves per atom.

There are several convergence criteria that must be addressed: the cutoff in the Fourier expansion of the charge density, the number of shells of vectors \mathbf{R}_L required to evaluate the Madelung energy, the mesh of \mathbf{k} points used to sample the band-structure energy, the exponents used in the Gaussian basis functions, and the size of the supercell. These criteria are not independent of each other and several iterations are needed to generate satisfactory values. Having selected a basis and supercell, the first three are easily dealt with: The number of shells of lattice vectors, the terms in the Fourier expansion, and the number of \mathbf{k} points generated by a Monkhorst-Pack (MP) scheme²¹ are increased until the energy changes by less than 0.001 a.u. per atom.

TABLE I. Basis exponents (a.u.) for s and p Gaussian orbitals for Si, Ge, and O. AC refers to orbitals sited at atoms while BC refers to those sited at bond centers. (N, M) refer to numbers of orbitals placed at nuclei and at bond centers, respectively. Lattice parameters a_0 (Å), the bulk moduli B (GPa), found from the basis sets are also given.

Species (N, M)	Silicon		Germanium		Oxygen	
	(4,1)	(4,2)	(4,1)	(4,2)	(6,1)	(6,2)
AC	0.1454	0.1272	0.1499	0.1509	0.2043	0.2815
	0.5002	0.3938	0.3747	0.4008	0.4339	0.5470
	1.2102	1.1592	0.9369	0.9018	0.9409	1.1665
	3.5712	3.1164	2.3422	2.4433	2.2011	2.5534
					4.7881	5.3166
				10.3587	11.4959	
BC	0.1946	0.1474	0.1632	0.1435	0.4624	0.2081
		0.3838		0.3824		0.4238
a_0 (calc.)	5.390	5.394	5.579	5.568		
B (calc.)	99.5	94.3	76.3	74.2		
a_0 (obs.)		5.431 ^a		5.658 ^b		
B (obs.)		97.9 ^a		77.2 ^b		

^aReference 77.

^bReference 78.

The Fourier transform of the charge density includes reciprocal-lattice vectors \mathbf{g} corresponding to kinetic energies up to 80 a.u. for Si and Ge, and 300 a.u. when oxygen is included in the cell. The large cut offs arise from the use of the BHS pseudopotentials and the lack of an occupied core p orbital for oxygen. Most calculations used 64-atom supercells and MP-2³ \mathbf{k} -point sampling. Several calculations were carried out in 216-atom supercells using only the MP-1³ scheme.

The convergence criteria involving the number of Gaussian exponents and the size of the supercell are more problematic. The wave-function basis consists of N Gaussian s and p orbitals, each specified by an exponent and located at the nuclei, and M similar orbitals located at each bond center to simulate the effect of higher-order angular momentum functions like d orbitals. The Gaussian exponents for Si, O, and Ge were found by minimizing the energy of a cell containing bulk material or a disiloxane molecule. The exponents were selected in the range between 0.1 and 3.6 a.u. by using a Metropolis-like algorithm. All the exponents used are given in Table I.

The table also shows that the calculated lattice parameters and bulk moduli for Si and Ge lie within 1% of the experimental values and that these structural parameters have converged for the smallest (4, 1) basis set. As a test, the structure of α quartz was also evaluated and the lattice parameters found to be within 0.6% of the observed values with the (4, 1) Si and (6, 1) O basis.

The energy, however, is much more sensitive to the basis and Table II shows its variation with different (N, M) values. Here the energies for primitive cells of Si and α quartz were evaluated using a MP-8³ sampling mesh and fixed-cell parameters equal to the converged values. It is clear that for the (4, 1) Si basis, the absolute energy per atom of bulk Si is in error by as much as 0.05 eV. Similarly, the Si (4, 1) and O

(6, 1) basis produces an error in the total energy of a unit cell of quartz of 0.008 a.u. or 0.2 eV.

The absolute energy is, however, not of major concern. Of greater interest are the formation energies of defects and their relative energies. The formation energy of a neutral defect is given by

$$E_f = E_D - \sum_i n_i \mu_i, \quad (1)$$

where E_D is the total energy of the supercell containing the defect and composed of n_i atoms of species i whose chemical potential is μ_i . The chemical potentials for Si and Ge are simply the energies per atom in the bulk phase. When dealing with oxygen defects in Si, we take μ_O to be given by the energy of an oxygen atom in α quartz, namely $\mu_O = (E_{3\text{SiO}_2} - 3\mu_{\text{Si}})/6$. A similar equation involving GeO_2 gives the chemical potential for oxygen in Ge. The formation energy then gives the equilibrium density of oxygen atoms in Si (Ge) when in equilibrium with SiO_2 (GeO_2).

The chemical potentials vary substantially with the basis as discussed above but the formation energies E_f of defects

TABLE II. Total energies (a.u.) for bulk Si and α quartz. The formation energy (eV) for an interstitial oxygen center was evaluated using Eq. (1), and is given in the right-hand column.

Basis		$E_{2\text{Si}}$	$E_{3\text{SiO}_2}$	$E_f(\text{O}_i)$
Si	O			
(3,0)	(6,0)	-7.8623	-108.1744	1.989
(3,1)	(6,1)	-7.9187	-108.4906	1.973
(4,1)	(6,1)	-7.9271	-108.5423	1.809
(4,2)	(6,2)	-7.9309	-108.5485	1.817
(4,3)	(6,3)	-7.9317	-108.5502	1.820

TABLE III. Energy per silicon atom and formation energy of O_i in Si (eV), evaluated in several supercells and sets of special \mathbf{k} -points. scN , $fccN$, and $bccN$ refer to simple cubic, fcc-centered-cubic, and body-centered-cubic lattices containing N Si atoms; n denotes the MP- n^3 sampling grid used.

Supercell	n	E_{Si}	$E_f(O_i)$	
			Calc. ^a	Calc. ^b
sc64	1	-107.7433	1.06	
fcc128	1	-107.7577	1.38	1.1
sc216	1	-107.8393	1.66	
bcc32	2	-107.8452	1.83	1.8
sc64	2	-107.8534	1.81	
sc8	20	-107.8549		

^aThis work.

^bReference 37.

calculated using a consistent basis are much less sensitive. This is illustrated in Table II which shows that E_f for interstitial oxygen in Si has converged to within 10 meV, for the (4, 1) Si and (6, 1) O basis. These calculations used 64 Si cells and MP-2³ sampling.

We now discuss the effect of different-sized supercells and sampling schemes. For this the basis was fixed to be Si (4, 1) and O (6, 1) and the unit-cells volume was relaxed. Table III shows that using a single \mathbf{k} point at Γ in a 64 Si atom cell gives an error in the energy per atom of about 0.1 eV but this decreases to about 0.0015 eV for an MP-2³ scheme.²¹ Thus in 64-atom cells, we invariably used this scheme. The MP-1³ sampling scheme was only used in 216-atom cells. Also shown is the formation energy of O_i . Here it is clear that the use of MP-1³ sampling gives poor energies except in the largest 216-atom cells.

To check the effect of the size of the supercell on the defect, the volume of the cell was relaxed. Calculations were first carried out using cells with the lattice constant found for pure Si and Ge crystals, i.e., 5.39 Å and 5.58 Å, respectively. However, as oxygen defects exert strong compressive effects, the energy is reduced by expanding the lattice. Whereas each defect gives a finite volume change—irrespective of the volume of the supercell—the fractional volume change should vanish in the limit of large cells. The magnitude of this change is then a measure of the sensitivity to cell size.

The vibrational modes were calculated from the energy second derivatives between the oxygen and surrounding atoms. Other second derivatives between host atoms were usually evaluated from a Musgrave-Pople potential derived previously.²² However, the O-related local mode observed in Si at 517 cm⁻¹, and lying just below the Raman frequency, is found to be sensitive to the movement of second shell Si atoms and, accordingly, second derivatives involving these atoms were also evaluated for this defect.

The dependence of the structure and the vibrational modes on pressure have also been investigated. To achieve this, the energy of the defect was calculated in cells of different volume V and the corresponding pressures P fitted to the Birch-Murnaghan equation of state.²³ Here,

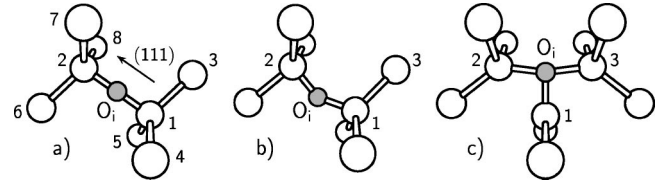


FIG. 1. D_{3d} (a), C_{1h} (b), and Y -lid (c) configurations for interstitial oxygen.

$$P = \frac{3}{2}B \left[\left(\frac{V_0}{V} \right)^{7/3} - \left(\frac{V_0}{V} \right)^{5/3} \right] \times \left\{ 1 + \frac{3}{4}(B' - 4) \left[\left(\frac{V_0}{V} \right)^{2/3} - 1 \right] \right\}, \quad (2)$$

V_0 is the volume of the cell with zero pressure, B the isothermal bulk modulus, and B' its isothermal pressure derivative.

To calculate the activation energy for the diffusion of O_i and O_{2i} , the saddle point lying on the diffusion pathway between translationally equivalent sites must be found. This can be achieved by relaxing the cell subject to some constraint preventing the defect from returning to its equilibrium site. In some cases this can be done by constraining the symmetry of the defect and in others by imposing algebraic constraints on bond lengths in a way described previously.²⁴ For example, when considering the diffusion of interstitial oxygen in Si, then with reference to Figs. 1(b) and 1(c), the oxygen atom must break its bond with 2 and make a bond with 3. At the same time, the Si atom 1 breaks a bond with 3 and makes one with 2. One might suppose that at the saddle point, the bonds between O_i and the atoms 2 and 3 are equal in length, as well as the 1-2 and 1-3 bonds. Appropriate constraints are then

$$c_1 = |\mathbf{R}_O - \mathbf{R}_3|^2 - |\mathbf{R}_O - \mathbf{R}_2|^2,$$

$$c_2 = |\mathbf{R}_1 - \mathbf{R}_3|^2 - |\mathbf{R}_1 - \mathbf{R}_2|^2,$$

with c_1, c_2 being zero at the midway point. All the atoms in the cell are relaxed subject to c_1, c_2 taking specific values. Using this procedure, the configuration energy surface can be found as a function of c_1 and c_2 and the barrier estimated by interpolation.²⁴ Previously this method was used to demonstrate that the Y -lid configuration of Fig. 1(c) is the saddle point for the diffusive step.²⁵

The stress tensor of O_i , say, can be calculated by first relaxing the volume of a cubic cell containing an oxygen atom in any alignment. Then the atoms of the cell and the cube axes are displaced by $\Delta R_l = \sum_m \epsilon_{lm} R_m$ and the atoms relaxed within the deformed cell. Care must be taken to include all inequivalent \mathbf{k} vectors. The components of the B tensor are then found by repeating the calculation for a number of independent strains. The principal values and directions of the tensor are then evaluated by diagonalization.

III. INTERSTITIAL OXYGEN

A. Introduction

Interstitial oxygen is known to lie near a bond-centered site with equal Si-O bonds and the static defect can, in prin-

TABLE IV. Relative energies (in meV) and structural details of configurations for O_i in Si or Ge (denoted by X).

	Si				Ge			
	C_2	C_1	C_{1h}	D_{3d}	C_2	C_1	C_{1h}	D_{3d}
E_{rel}	0	9	1	13	0	12	3	106
X-O, Å	1.62	1.61	1.62	1.61	1.73	1.73	1.73	1.71
X-O-X (deg)	158	166	157	180	143	146	144	180

ciple, assume either C_1 , C_{1h} , C_2 , or D_{3d} symmetry. The different symmetries depend on the position of O with respect to the back-bonded Si atoms as shown in Figs. 1(a) and 1(b). In D_{3d} , the O atom lies at the bond center. The defect possess several bands of vibrational modes which, at low temperatures ($T < 40$ K), lie around 30, 517, 1136, and 1750 cm^{-1} . Although these bands have been intensively investigated in the last 50 years, only those at 30 and 1136 cm^{-1} are clearly understood.^{26–28}

The first arises from the motion of the O atom in a plane normal to the Si-O-Si direction. These modes were analyzed in terms of an empirical potential which led to the conclusion that the equilibrium Si-O-Si angle is 164° and that the energy barrier to the bond-center site is of the order of 10 meV.²⁶ Further investigations have lowered the barrier to about 1 meV so that the O atom tunnels between equivalent sites leading to an effective D_{3d} symmetry.²⁷ The 1136- cm^{-1} (A_{2u}) band arises from an asymmetric stretch of the two Si-O bonds, while the 517- cm^{-1} band, lying near the Raman line of bulk Si, has been assigned either to a symmetric stretch mode (A_{1g}) or to an E_u mode with little amplitude on the O atom. The latter is required as the mode is insensitive to the oxygen mass.

The 1750- cm^{-1} band has been attributed to a combination of the 1136- cm^{-1} mode and an infrared (IR) inactive band around 600 cm^{-1} .²⁷ This has recently been supported by the discovery of a new oxygen-related band at 648.2 cm^{-1} assigned to a combination between a weak, or inactive, mode at ~ 618 cm^{-1} and the low-energy band at 30 cm^{-1} .²⁹

In the case of Ge, the situation is less clear. Here, interstitial oxygen produces three absorption bands at ~ 1 , 860, and 1260 cm^{-1} .^{30,31} These can be considered as analogs of the 30-, 1136-, and 1750- cm^{-1} bands in Si. Gienger *et al.*³⁰ suggested that in Ge, the Ge-O-Ge angle is smaller than in Si and the low-energy excitations are between different axial angular momentum states of a rigid buckled Ge-O-Ge rotator as shown in Fig. 1(b). It is thus expected that the barrier for moving the O atom to the bond-center site is larger in Ge than Si.

Previous modeling studies in Si have determined both the structure of the defect and two high-frequency O-related fundamentals.^{32,33} These were located at 1104 and 554 cm^{-1} and assigned to the asymmetric and symmetric modes of the buckled Si-O-Si unit, respectively. The modes related to E_u fell below the Raman and were hidden by the lattice modes.

Calculations carried out in Ge gave a symmetric stretch mode around ~ 400 cm^{-1} ,³⁴ but no band near the Raman edge was reported. Again, the 1260 cm^{-1} band is assigned to a combination between the symmetric (~ 400 cm^{-1}) and antisymmetric (860 cm^{-1}) modes.

B. Theoretical results

Table IV shows the relative energies and structure of the defect when confined to C_2 , C_1 , C_{1h} , and D_{3d} symmetry calculated in a 64 Si or Ge atom supercell. It is clear that in Si, there is very little energy difference between all the structures consistent with a tunneling model. In Ge, however, the bent Ge-O-Ge configuration, with an angle about 144° , is preferred with about 0.1 eV barrier to the D_{3d} structure. In these calculations the cell size was fixed using the calculated host lattice parameter a_0^{eq} equal to 5.39 Å in Si, and 5.58 Å in Ge. However, the high concentration of defects ($\sim 10^{21}$ cm^{-3}) may result in a substantial volume change and this was investigated by allowing the cell volume to relax. Figure 2(a) shows the variation in the total energy when the lattice parameter is varied. The energy difference between the C_2 and D_{3d} structures vanishes for lattice dilations larger than 0.5% but the C_2 structure is increasingly favored under compression. The decrease in the energy of the cell when the lattice parameter is varied in this way is ~ 30 meV in Si, while the bulk modulus is shifted downwards by $\sim 2\%$ in Si and upwards by 0.5% in Ge. The effect of this concentration of oxygen is to increase the lattice parameter by 0.3% in both Si and Ge. Since the density of oxygen is 1/64 of that of Si, then this corresponds to an increased lattice parameter of $\epsilon[\text{O}]/[\text{Si}]$, where ϵ is found to be 0.19. This agrees precisely with x-ray data giving the same value of ϵ .^{35,36}

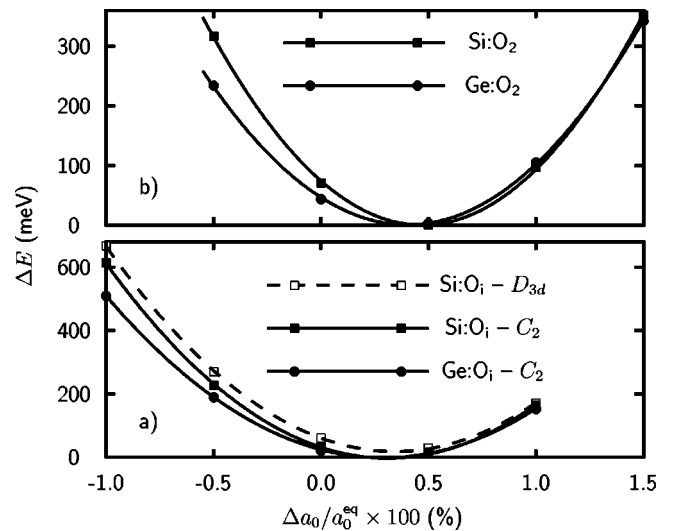


FIG. 2. Relative energies of (a) interstitial oxygen in Si (squares) or Ge (circles), and (b) staggered dimers in Si (squares) or Ge (circles) versus the lattice parameter of a 64-atom cell. a_0^{eq} refers to calculated Si and Ge bulk lattice constants of 5.39 Å and 5.58 Å, respectively.

TABLE V. Formation energies (eV) for the single oxygen and dioxygen centers in Si and Ge. fccN, scN, bccN, and ttrN denote face-centered-cubic, simple-cubic, body-centered-cubic, and tetragonal cells with N Si or Ge atoms. In the third column, n denotes the BZ sampling scheme utilized.

		MP- n^3	Cell	O _i	O ₂ st	O ₂ ^{sk}	O ₂ ^{dy}	VO	VO ₂
This work	Si	1	sc216	1.66	2.88				
	Si	2	sc64	1.81	3.08	3.27	4.79	3.85	3.93
	Si	2	ttr96		3.04				
Pesola <i>et al.</i> ^a	Si	1	fcc128	1.1	2.0	2.1			
	Si	2	sc64					3.7	3.7
	Si	2	bcc32	1.8	3.0	3.4			
This work	Ge	2	sc64	1.19	1.76	2.31	3.61	3.05	2.94
	Ge	2	ttr96		1.73				

^aReference 37.

Table V gives the formation energy of O_i in different sized cells. The calculated value lies between 1.66 and 1.81 eV in Si, somewhat larger than found by a plane-wave method.³⁷ Assuming the solubility is given by $N_{\text{BC}}e^{-E_f/kT}$, where N_{BC} is the density of bond-center sites, we obtain an equilibrium solubility between 6×10^{16} and 2×10^{17} cm⁻³ at 1300 °C. This compares with a measured solubility of about 3×10^{18} cm⁻³ which corresponds to a formation energy of interstitial oxygen of around 1.4 eV.²⁵ These estimates have ignored the vibrational entropic contributions.

The O atom with C_2 symmetry is displaced by 0.31 Å from the BC site in a [110] direction leading to a Si-O-Si angle of 158°. The Si-O length is 1.62 Å, slightly longer than that in the D_{3d} configuration. Table IV shows that similar geometries are obtained in the C_1 and C_{1h} configurations.

The calculated LVM's for the C_2 and D_{3d} structures and their isotopic shifts are shown in Table VI. These are compared with values obtained previously^{32,37,34} and the observed modes.^{38,29,39} The frequencies for the combination bands were obtained by summing the fundamental modes.

There are four fundamental modes for the C_2 defect. Asymmetric (B) and symmetric (A) stretch modes lie at 1108 and 621 cm⁻¹ and a near degenerate pair of modes lie at 518 cm⁻¹. The latter are split by 0.2 cm⁻¹ and lie below the 526-cm⁻¹ Raman frequency given by the Musgrave-Pople potential. They are recognized by their large amplitude on the two shells of Si neighbors to oxygen and arise from the compression of the back bonds by oxygen, but the oxygen atom does not participate in their motion. This follows from the insensitivity of these two lower modes to the oxygen mass (Table VI). However, a shift of 1 cm⁻¹ occurs when one of the neighboring Si atoms is replaced by ³⁰Si. In D_{3d} , the two highest modes have A_{2u} and A_{1g} symmetry. The latter is infrared inactive and implies that its analog in C_2 at 621 cm⁻¹ would be only weakly IR active. The lower pair of modes have E_u symmetry. The vibrational modes associated with these frequencies are shown in Figs. 3(a)–3(c).

The calculated LVM's for both C_2 and D_{3d} symmetries are similar to each other and in good agreement with the experimental data. This is especially true for the mode around 621 cm⁻¹ which has been detected as a partner in two combination bands.^{27,29} Thus, there is nothing in the observed or calculated modes that allows the symmetry of

the defect to be unambiguously identified. As described above, the D_{3d} model has been singled out as it can explain the fine structure of the 30-cm⁻¹ band. However, this band is too low in frequency to be accurately modeled using *ab initio* methods. Nevertheless, the effect of pressure on the high-frequency modes allows us to discriminate between these models.

Figure 4 shows the LVM's as a function of pressure. This dependence can be expressed through either the isotropic piezospectroscopic tensor element A_1 , given in Table VII, and appropriate for a trigonal defect, or through the Gruneisen parameter, $\gamma = -\partial \ln \omega / \partial \ln V$. We find that, for the D_{3d} structure, A_1 is positive for all LVM's—in agreement with experiment at low pressures.^{40,29,31,34} The large difference between the values of A_1 for the 1136-cm⁻¹ band found by uniaxial and hydrostatic stress experiments is in part due to the nonlinear fit employed in the latter.⁴¹

However, A_1 is negative for the C_2 structure as the buckling increases with pressure and leads to slightly dilated Si-O bonds. Experimentally, the asymmetric stretch mode decreases with increasing hydrostatic pressures beyond about 1 GPa.⁵ This can be explained as a change from a D_{3d} configuration at low pressures to the buckled form for pressures ~ 1 GPa.

The stress tensor for O_i in Si has been calculated as described above. We find the principal values for the D_{3d} structure are $B_3 = -2B_2 = -2B_1 = -10.71$ eV with the principal direction of B_3 along the C_3 axis. The negative value of B_3 indicates that the defect is compressive along the Si-O-Si bond as expected. These are in fair agreement with the experimental results of $B_3 = -2B_2 = -2B_1 = -15.2$ eV.⁶

In summary, the calculations find that interstitial oxygen in Si, at normal pressures, is likely to tunnel between bent Si-O-Si configurations with effective D_{3d} symmetry. In this configuration, there are two localized fundamentals at 1184 (A_{2u}), 619 (A_{1g}), and an E_u resonance at 519 cm⁻¹. The frequency of the modes increase with pressure. However, for a critical pressure, the energy difference between the C_2 and D_{3d} configurations increases, and tunneling no longer occurs. In this case the O atom could still rotate around the (111) axis with the asymmetric stretch mode decreasing with increasing pressure.

TABLE VI. Calculated LVM's (cm^{-1}), and their downward isotopic shifts for different configurations for O_i in Si and Ge. Results of previous calculations are given along with observed modes. Two-phonon modes are estimated by a simple summation of asymmetric and symmetric fundamentals.

	Mode	$^{28}\text{Si } ^{16}\text{O } ^{28}\text{Si}$	$^{30}\text{Si } ^{16}\text{O } ^{28}\text{Si}$	$^{28}\text{Si } ^{18}\text{O } ^{28}\text{Si}$	$^{30}\text{Si } ^{18}\text{O } ^{28}\text{Si}$
Calc. ^a	$A+B$	1729	14	53	66
	B	1108	4	50	54
C_2	A	621	10	3	12
	A,B	518	2	0	2
Calc. ^a	$A_{1g}+A_{2u}$	1803	14	54	68
	A_{2u}	1184	4	55	58
D_{3d}	A_{1g}	619	10	0	10
	E_u	519	1	0	1
Calc. ^b	B	1098		50	
	A	630		2	
Calc. ^c	A	1104		53	
	B	554		1	
Observed ^d		1748.6	12.2	52.6	
		1136.4	3.7	51.4	55.2
		~ 618	9.5	~ 0	
		517.8		0.0	
	Mode	$^{70}\text{Ge } ^{16}\text{O } ^{70}\text{Ge}$	$^{74}\text{Ge } ^{16}\text{O } ^{74}\text{Ge}$	$^{70}\text{Ge } ^{18}\text{O } ^{70}\text{Ge}$	$^{74}\text{Ge } ^{18}\text{O } ^{74}\text{Ge}$
Calc. ^a	$A+B$	1248	8	55	63
	B	847	2	44	46
C_2	A	401	6	11	17
Calc. ^e	$A+B$	1293	8		
	B	878	3		
	A	416	6		
Observed ^f		1274.0	8.3		
		862.91	1.01	43.28	45.45
		412.1 ^g	7.3 ^g		

^aThis work.

^bReference 37.

^cReference 32.

^dReference 38, except the 618-cm^{-1} band from Ref. 29.

^eReference 34.

^fReference 39.

^gThis frequency was calculated by assuming the existence of a combination mode $A+B$ at 1274.0 cm^{-1} .

In germanium, the D_{3d} structure has energy 0.1-eV higher than the others which are all degenerate (see Table IV). The formation energy for O_i is lower than in Si and hence the solubility of oxygen in Ge in equilibrium with GeO_2 should be higher. This suggests that precipitation of oxygen in Ge should have less tendency to occur. The Ge-O-Ge angle is 143° and the oxygen atom lies 0.55 \AA away from the BC site with the Ge-O bond length at 1.73 \AA . The energy barrier to the D_{3d} case suggests that tunneling cannot occur, but the oxygen atom may rotate around the (111) axis. Table VI gives the calculated and experimental LVM's. Two fundamental LVM's lie at 847 and 401 cm^{-1} and represent asymmetric and symmetric stretch modes of the Ge-O-Ge buckled unit. In general, these results are in agreement with previous investigations.^{42,32,34,37,43} In contrast with Si, these frequencies do not drop with increasing pressure and no mode

around the Raman frequency occurs. The difference in behavior is probably due to the very different bond angle in the two materials.

IV. DIFFUSION OF INTERSTITIAL OXYGEN

The activation energy for an oxygen atom hopping between neighboring bond centers in Si has been measured by stress-induced dichroism⁴⁴ to be 2.56 eV and the same barrier was found for the long-range diffusion of oxygen as measured by secondary-ion mass spectrometry.⁷ In Ge, the diffusion energy is 2.08 eV .⁴⁴ The similarities in the oxygen diffusion energies in Ge and Si suggests an identical diffusion mechanism.

The saddle point for hopping between bond centers has been found to be the Y -lid configuration with C_{2v} symmetry

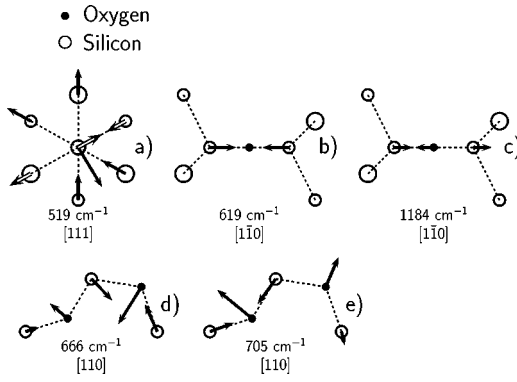


FIG. 3. Normal coordinates of the vibrational modes for O_i in Si [(a), (b), and (c)] and for the dimer modes at 666 and 705 cm^{-1} [(d) and (e)]. The two components of the E_u mode in (a) are distinguished by filled and outlined arrows. The 666 cm^{-1} mode in (d) has a small induced dipole moment arising from the movements of the oxygen atoms which are out of phase with each other. The normal to the projected plane is given in each case.

and shown in Fig. 1(c).²⁴ In this configuration, both the O atom and the Si_1 neighbor are threefold coordinated.

In the present paper, the energy of the Y lid is calculated by relaxing 32, 64, and 128 atom cells with the symmetry maintained to be C_{2v} . The lattice parameter was again taken to be given by the calculated bulk value. We found that in Si this energy is 2.1 to 2.2 eV higher than the C_2 structure when using cells with these sizes. Allowing the volume of the cell to relax lowered the energy of the Y -lid configuration by 10 meV. This has a negligible effect on the diffusion energy. If the O atom is slightly perturbed, then upon relaxation without any constraint, it returns to the stable C_2 site. Thus the calculated diffusion energy is about 2.2 eV compared with an experimental value of 2.5 eV. This may be compared with previous estimates of 2.8,²⁵ 1.8,⁹ 2.2,⁸ and 2.0 eV.¹⁰

In a similar way, the energy of the Y -lid structure in Ge is found to be 1.70 eV above its ground state. In both materials, the diffusion barrier is underestimated by about 0.3 eV. This may result from inadequacies in local density-functional theory or slow convergence in cell size or basis.

V. INTERSTITIAL OXYGEN DIMERS

A. Introduction

When oxygen-rich Si is heated to around 450 °C, a family of thermal double donors are formed and it is known that the process whereby the early thermal double donors are trans-

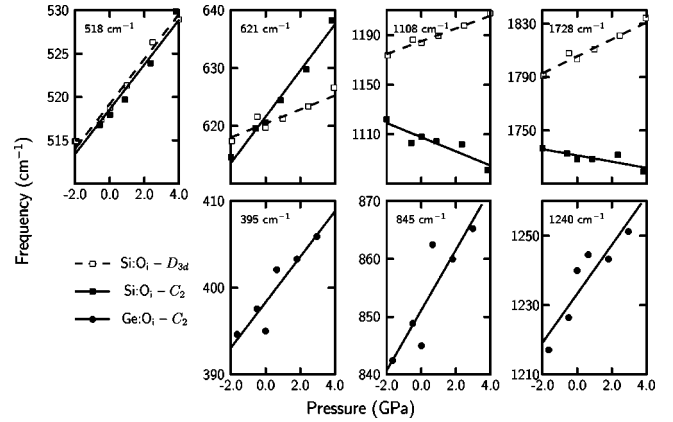


FIG. 4. Effect of pressure on LVM's of interstitial oxygen in Si (upper row) and Ge (lower row).

formed into later ones is activated with an energy of ~ 1.8 eV.^{45,25} If the conversion is due to oxygen aggregation, then this implies that some oxygen species can diffuse at a much faster rate than isolated oxygen atoms. Moreover, careful studies of the loss of the intensity in the 1136- cm^{-1} band with prolonged anneals below 500 °C strongly suggest a fast diffusing dimer. This makes the dimer species a key entity in kinetic studies of oxygen aggregation in Si.^{46,47}

A suggestion for a fast diffusing oxygen-related species was made by Gösele and Tan⁴⁸ and attributed to an O_2 molecule. However, later calculations indicated that the molecule was less stable than an oxygen dimer where both oxygen atoms are tilted along the $[110]$ direction with respect to each other [see Fig. 5(a)].⁹ Here the oxygen atoms were found to be bound by 1 eV.

Subsequent infrared-absorption studies have identified the LVM's of an oxygen dimer. These lie at 1060, 1012, 690, and 556 cm^{-1} . The intensities of these modes vary with the square of the O_i concentration¹⁵ and in the ^{16}O - ^{18}O mixed isotopic case, unique modes are detected demonstrating the presence of two oxygen atoms that are dynamically coupled. The two oxygen atoms, O_1 and O_2 , must be inequivalent as these unique modes are only found in one of the $^{16}\text{O}_1$ - $^{18}\text{O}_2$ combinations. This unusual behavior is reflected in the intensities of the modes.¹⁵

Further investigations suggested that a second dimer, called the skewed [see Fig. 5(b)] because a Si-Si bond separates the Si-O-Si units which lie in different (110) planes, is energetically competitive with the staggered dimer.^{14,15} Previously, we found, using the cluster method, that the skewed dimer possesses LVM's closer to the experimental values

TABLE VII. Calculated values for the isotropic piezospectroscopic tensor element A_1 ($\text{cm}^{-1} \text{GPa}^{-1}$) for local modes of O_i along with the experimental data. Grüneisen parameters for each mode are between parentheses.

Mode	Si: C_2		Si: D_{3d}		Obs.	Ge: C_2	
$A_{2u} + A_{1g}/A + B$	-0.78	(-0.13)	2.28	(0.37)		3.68	(0.50)
A_{2u}/B	-2.11	(-0.55)	1.81	(0.45)	0.77 ^a , 0.2 ^b	1.64	(0.44)
A_{1g}/A	1.33	(0.62)	0.47	(0.22)		0.82	(0.50)
$E_u/A, B$	0.86	(0.47)	0.84	(0.47)	~ 1.1 ^b		

^aReference 5.

^bReference 26.

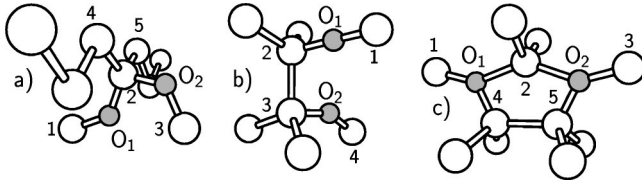


FIG. 5. Schematic structure of oxygen dimers. (a) Staggered (O_2^{st}), (b) skewed (O_2^{sk}), and (c) double- Y lid (O_2^{dy}). Oxygen atoms are gray.

than those of the staggered dimer. The converse was, however, found by Pesola *et al.*¹⁶ To address this problem, the LVM's have been reevaluated using the supercell method. The temperature dependence of the two highest modes is anomalous as their frequencies decrease with temperature. We shall show that this can be explained by an increased bucking which occurs under pressure.

In Ge, interstitial oxygen dimers have not been identified and few theoretical studies have been performed.⁴⁹ However it is reasonable to expect that oxygen clustering in Ge will start with the dimer formation as in Si.

B. The oxygen dimer

The structure, energetics, and vibrational modes of the staggered, skewed, and double- Y -lid dimers shown in Fig. 5 were calculated mainly in 64-atom supercells, although some calculations used 96- or 216-atom supercells.

Table V gives the formation energy of these dimers. Cells with 64 and 96 silicon atoms give values within 0.04 eV, suggesting that they are sufficiently large. The formation energy calculated in the largest 216 cell is not necessarily more accurate than found in the 64- or 96-atom cells as only one \mathbf{k} point was used to sample the band structure in this case. Figure 2(b) demonstrated that the effect of allowing the cell

volume to relax is negligible, consistent with the view that 64-atom cells are sufficiently large.

The binding energies for the dimers obtained from the formation energies in Table V are given in Table VIII where they are compared with previous studies. The binding energy of the oxygen atoms in the staggered dimer is found to be about 0.5 and 0.6 eV in Si and Ge, respectively. An experimental estimate in Si is about 0.3 eV.¹⁴ The skewed configuration is less favored by about 0.2 eV in Si, but is only marginally bound in Ge. Table IX gives structural details of the dimers.

The symmetric double- Y -lid dimer is found to be energetically disfavored by about 1.2 eV relative to two isolated oxygen atoms in both Si and Ge. This is in contrast with previous work on this structure in Ge which found this structure to be bound with an energy of 0.7 eV.⁴⁹ Nevertheless, the 1.2 eV required to form the symmetric double- Y lid suggests that the dimer can diffuse with at least this activation energy which is lower than the barrier for single oxygen diffusion. This is a subject we shall investigate in the next subsection.

We also investigated the O_2 molecule lying at a T site. This oxygen dimer is not stable, being 6.03-eV higher in energy than the staggered dimer. We discuss the stability relative to VO_2 in Sec. VII and now turn to the vibrational modes of the dimers.

The LVM's for the staggered and skewed dimers were found by evaluating the energy second derivatives between the O atoms and their Si neighbors. They are given in Table X along with the observed modes. There are five modes of the dimer but only four have been detected. The calculated modes are within 40 cm^{-1} of the observed ones. However, of great importance is their isotopic shifts. For the staggered dimer, when the oxygen atom labeled O_2 in Fig. 5 is replaced by its ^{18}O isotope, the 1017-cm^{-1} mode drops only by

TABLE VIII. Binding energies (eV) for interstitial dioxygen centers in Si and Ge. fcc N , sc N , bcc N , and ttr N denote face-centered-cubic, simple-cubic, body-centered-cubic, and tetragonal cells with N Si or Ge atoms. In the third column, n denotes the BZ sampling scheme utilized.

	Crystal	MP- n^3	Cell	O_2^{st}	O_2^{sk}	O_2^{dy}
This work	Si	1	sc216	0.44		
	Si	2	sc64	0.54	0.35	-1.17
	Si	2	ttr96	0.58		
Pesola <i>et al.</i> ^a	Si	1	fcc128	0.2	0.1	
	Si	2	bcc32	0.6	0.2	
Chadi ^b	Si		bcc32	0.4		
Needels <i>et al.</i> ^c	Si		fcc16-sc64	1.0		
This work	Ge	2	sc64	0.62	0.07	-1.23
	Ge	2	ttr96	0.65		
Chadi ^b	Ge		bcc32			0.7

^aReference 37.

^bReference 49.

^cReference 9.

TABLE IX. Bond lengths (\AA) and angles (deg) for oxygen dimers in Si and Ge (represented by X), shown in Fig. 5.

Crystal dimer	Si			Ge		
	Staggered	Skewed	Double-Y lid	Staggered	Skewed	Double-Y lid
O ₁ -X ₁	1.66	1.61	1.75	1.77	1.73	1.86
O ₁ -X ₂	1.64	1.62	2.11	1.74	1.74	2.19
O ₁ -X ₄			1.75			1.85
O ₂ -X ₂	1.63		2.11	1.74		2.19
O ₂ -X ₃	1.67	1.63	1.75	1.77	1.75	1.86
O ₂ -X ₄		1.63			1.74	
O ₂ -X ₅			1.75			1.85
X ₂ -X ₃		2.29			2.39	
X ₄ -X ₅			2.37			2.57
X ₁ -O ₁ -X ₂	130	166	146	125	147	147
X ₁ -O ₁ -X ₄			131			128
X ₂ -O ₂ -X ₃	127		146	124		147
X ₃ -O ₂ -X ₄		148	131		138	128

TABLE X. Calculated LVM's (cm^{-1}) and their downward isotopic shifts for staggered and skewed dimers (O₂st and O₂^{sk}, respectively) in Si and Ge, along with the experimental observations.

	¹⁶ O ₁ , ¹⁶ O ₂		¹⁶ O ₁ , ¹⁸ O ₂		¹⁸ O ₁ , ¹⁶ O ₂		¹⁸ O ₁ , ¹⁸ O ₂	
	Calc. ^a	Calc. ^b						
Si:O ₂ st	1017	1033	2	1	28	40	46	46
	984	984	41	42	17	6	42	42
	705	697	4	4	9	6	14	11
	666	661	9	6	3	3	10	8
	543	566	0	0	0	0	0	0
Si:O ₂ ^{sk}	1166	1104	0	1	52	52	53	50
	1094	1091	48	48	1	-3	49	50
	636	643	3	2	0	1	3	3
	624	627	1	1	0	2	1	3
	552	558	0	0	0	0	0	0
Observed ^c	1060		~0		39		48	
	1012		42		8		43	
	690		4		~4		10	
	556		~0		~0		0	
Ge:O ₂ st	784		8		17		41	
	749		32		23		38	
	517		8		11		22	
	466		13		9		18	
Ge:O ₂ ^{sk}	849		4		1		44	
	843		40		42		44	
	389		1		10		11	
	366		7		0		7	

^aThis work.^bReference 16.^cReference 15.

2 cm^{-1} but the 984- cm^{-1} mode drops by 41 cm^{-1} . These are in excellent agreement with observed drops of ~ 0 and 42 cm^{-1} , respectively. However, when O_i in Fig. 5 is replaced by ^{18}O , the 1017 cm^{-1} mode is expected to drop by about 40 cm^{-1} , bringing it close to the 984- cm^{-1} mode. The two modes then are in resonance and become coupled leading to shifts of 28 and 17 cm^{-1} in each mode. These are to be compared with observed shifts of 39 and 8 cm^{-1} . Clearly the degree of coupling is overestimated but is less than that found by the cluster method previously.

The calculated shifts in the 705- and 666- cm^{-1} modes are 14 and 10 cm^{-1} , respectively, and 0 cm^{-1} for the 543 cm^{-1} mode. These shifts are in reasonable agreement with shifts in the observed bands at 690 and 556 cm^{-1} .

In the skewed configuration, the modes are essentially decoupled and the frequencies too high. They resemble those of two isolated oxygen interstitials. This suggests that the observed modes arise from the staggered dimer.

Only one of the modes around 690 cm^{-1} has been detected probably because the transition moment in the other is very small. The displacements of the atoms are shown schematically in Figs. 3(d) and 3(e). Locating point charges at each O and neighboring Si atoms leads to an induced dipole moment which is three times greater in the 705- cm^{-1} mode than in the 666- cm^{-1} mode. This probably occurs as the displacements of the oxygen atoms are in phase in the 705- cm^{-1} mode and out of phase in the 666- cm^{-1} mode. We therefore assign the observed 690- cm^{-1} band to the higher frequency.

In Ge, the dimer modes are very similar to those in Si and the two high-frequency stretch modes are reduced by a factor of 0.77 from the asymmetric stretch mode of O_i while the lower pair are reduced by a factor of about 0.73. A band at 780 cm^{-1} detected in annealed electron-irradiated oxygen-doped Ge has been attributed to the dimer.⁵⁰ This band is shifted downwards by 23 and 41 cm^{-1} in ^{18}O - ^{16}O mixtures. The position of the dimer band and its isotopic shifts agrees with the calculated mode at 749 cm^{-1} which shifts 23 and 38 cm^{-1} with ^{18}O doping. However, further work is necessary to determine the other modes of the dimer. Further support for the assignment of this band to an oxygen aggregate comes from recent findings of a strong enhancement in thermal-donor concentrations consequent upon annealing irradiated material containing the 780- cm^{-1} band.⁵¹

The dimer modes in Si are observed to display an anomalous temperature dependence. Normally, the fundamental frequency of a defect increases with decreasing temperature resulting from strengthened bonds arising from the lattice contraction. However, the bands at 1012 and 1060 cm^{-1} shift downwards with temperature.¹⁵ To investigate this anomaly we decreased the lattice parameter in the 64-atom supercell containing the staggered dimer. The effect was to decrease further the Si-O-Si angles, i.e., increase their buckling, and reduce the asymmetric stretch modes as shown in Fig. 6. Thus, if the effect of lowering the temperature is simply to contract the lattice and impose a pressure on the dimer, then the upper two modes would decrease in frequency while the lower modes would increase. The same situation holds for the dimer in Ge—in contrast with what was found for O_i in this material. However, the band at 780 cm^{-1} , attributed to dimers in Ge, does not appear to

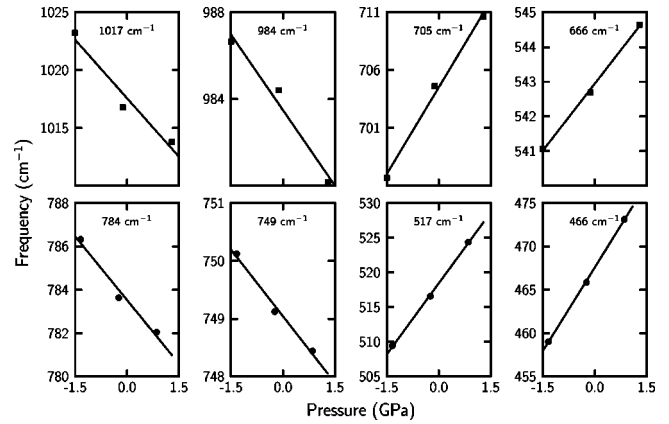


FIG. 6. Effect of pressure on LVM's of the staggered dimer in Si (upper row) and Ge (lower row).

shift anomalously with temperature. There clearly are two opposing effects at work: the first is an increased buckling which leads to a downward shift in frequency, and the second is the compression of the X-O bond lengths which lead to a frequency increase. In Si the first effect is dominant, but the second dominates in Ge.

C. Diffusion of the dimer

The activation energy for movement of the dimer was investigated using three different diffusion paths: (i) a correlated jump of both oxygen atoms from the staggered configuration through the asymmetric double-Y-lid structure of curve (i) in Fig. 7, (ii) a partial dissociation involving an asymmetric Y lid as in curve (ii) of Fig. 7, and a transition between the staggered and skewed dimers as proposed by Pesola *et al.*¹⁶ and shown in curve (iii) of Fig. 7. The migration energies were determined by relaxing the cell with constraints on the lengths of the O-X bonds as described earlier and shown in the figure.

Path (i) leads to a migration energy of 1.4 eV, (ii) leads to a similar barrier of 1.6 eV, although the complete diffusion event requires the oxygen atom at the left side to make a

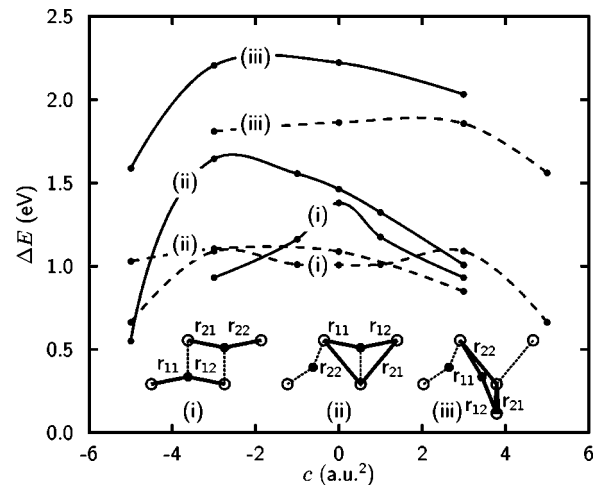


FIG. 7. Energies (eV) along three diffusion paths discussed in the text for oxygen dimers in Si (solid lines) and Ge (dashed lines). ΔE is the energy relative to a stable dimer. The x axis refers to the value of the constrained variables $c = \mathbf{r}_{11}^2 - \mathbf{r}_{12}^2 = \mathbf{r}_{21}^2 - \mathbf{r}_{22}^2$.

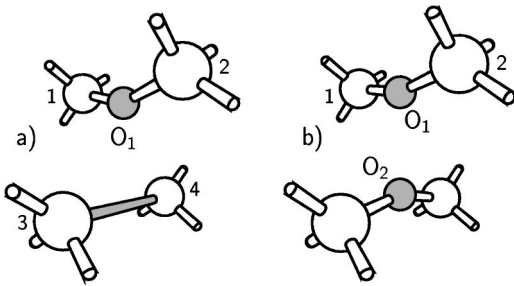


FIG. 8. The VO (left) and VO₂ (right) centers. In (a) the dark bond represents a reconstructed bond between Si or Ge atoms 3 and 4.

similar jump to reform the dimer. However, symmetry considerations require this second step to be equivalent to the first. Path (iii) is activated by a barrier of 2.2 eV, and resembles the diffusion of isolated interstitial oxygen.

One can rationalize these results by noting that in (i) both threefold-coordinated Si atoms labeled 1 in Fig. 1(c) are now bonded to the other O atoms. Similarly, in (ii) the tensile strain along [110] in the *Y* lid is offset by the presence of the second O atom. The effect of both these processes is to transport the dimer along [110] but both lead to a staggered dimer which tilts in the opposite direction. Before long-range migration can occur, the dimer must reorientate and point in the opposite direction. The energy barrier for this is found to be low: 0.38 eV in Si and 0.65 eV in Ge. Thus we conclude that the diffusion path probably occurs by the staggered dimer migrating along its [110] axis with a correlated jump of both oxygen atoms.

For Ge, Fig. 7 shows that the energy surface around the saddle-point is flatter than in Si. This is because the smaller Ge-O-Ge angle means that the oxygen atom is “closer” to the saddle point and consequently the “length” of the trajectory is shorter. In summary, the calculations demonstrate that oxygen dimers diffuse in Si and Ge with barriers about 0.8 and 0.6 eV, respectively, below the calculated barriers for O_{*i*}.

VI. SUBSTITUTIONAL OXYGEN: VO

A. Introduction

The vacancy oxygen (VO or A center) is one of the most common defects produced by room-temperature electron irradiation of Si or Ge containing oxygen.^{52,53,50} It is believed to form through trapping of mobile vacancies by interstitial oxygen atoms. The accepted structure is shown in Fig. 8(a) and involves a weak Si-Si reconstructed bond between the Si

atoms labeled 3 and 4. In Si, the defect has an acceptor level at $E_c - 0.17$ eV,⁵² while the corresponding defect in Ge has an acceptor level located at $E_c - 0.25$ eV.⁵⁴ The acceptor level of the defect in Si has been calculated previously by the cluster method to be $E_c - 0.13$ eV.⁵⁵

In Si, VO⁽⁰⁾ and VO⁽⁻⁾ are known to possess IR-active LVM’s with B_1 symmetry at 835 and 885 cm⁻¹, respectively.^{53,56} However, in Ge only one band at 620 cm⁻¹ has been attributed to the defect,⁵⁰ probably in the neutral state.

Previous theoretical work has successfully investigated the defect in Si, although the upward shift in the LVM for VO⁽⁻⁾ was not reproduced.^{57,37} Recent experimental work has assigned a combination band $A_1 + B_1$ around 1400 cm⁻¹, where A_1 is a symmetric stretching mode.^{58,59}

B. Results for the VO center

Table XI gives structural details of the neutral VO⁽⁰⁾ and charged VO⁽⁻⁾ defects in both Si and Ge as found in cells with 64 atoms. The O atom in both charge states moves away from the *T* site and bridges two host atoms. The length of the reconstructed bond increases from 3.26 Å in the neutral defect to 3.42 Å in the negatively charged center. This small change leads, as we shall show below, to a dramatic change in the piezospectroscopic tensor. Similarly, the Si-O bond length decreases on trapping an electron and this leads to an increase on the frequency of the oxygen stretch mode.

Table V gives the formation energies of the interstitial and neutral substitutional oxygen centers. It is clear that the formation energy of VO exceeds O_{*i*} by more than 2 eV, and thus the substitutional defect is only expected to be found at high temperatures or in the presence of a nonequilibrium concentration of vacancies produced, for example, by irradiation. Nevertheless, there is a strong binding between a vacancy and interstitial oxygen. The reaction energies are given in Table XII. Here a positive value indicates that the reaction is exothermic. This table shows there is a binding energy of about 1.6 eV between V and O_{*i*}. The formation energies for the vacancies in Si and Ge used in Tables V and XII were evaluated in 63-atom cells to be 3.61 and 2.20 eV, respectively, in good agreement with recent plane-wave calculations.^{60,61}

In the negative charge state, the O atom is displaced away from the reconstructed bond consistent with the idea that the additional electron is trapped in this bond and repels the negatively polarized O atom. This movement leads to a compression of the bonds around O implying an enhancement in the LVM as shown in Table XIII.

TABLE XI. Bond lengths (Å) and angles (degrees) for VO and VO₂ centers in Fig. 8. *X* is Si or Ge and *V* denotes the center of the vacancy.

	Si			Ge		
	VO ⁽⁰⁾	VO ⁽⁻⁾	VO ₂	VO ⁽⁰⁾	VO ⁽⁻⁾	VO ₂
O ₁ -X ₁	1.70	1.68	1.67	1.79	1.79	1.77
X ₁ -X ₂	3.26	3.27	3.28	3.45	3.46	3.48
X ₃ -X ₄	3.32	3.42	3.28	3.36	3.36	3.48
X ₁ -O-X ₂	150	154	158	150	152	158
O-V	1.05	1.08	1.23	1.13	1.14	1.31

TABLE XII. Reaction energies (eV) of vacancy-oxygen-hydrogen defects in Si and Ge. Negative values indicate endothermic behavior.

Reactants	→	Products	Silicon		Germanium
			Calc. ^a	Calc. ^b	Calc. ^a
$V+O_i$	→	VO	1.57	1.4 ^c , 0.8 ^d	0.36
O_i	→	VO+Si	-2.04		-1.86
$V+O_{2i}$	→	VO ₂	2.76	2.6 ^c , 1.6 ^d	1.04
O_{2i}	→	VO ₂ +Si	-0.85		-1.18
O_i+VO	→	VO ₂	1.73	1.8 ^c , 1.0 ^d	1.30
$VO+O_{2i}$	→	VO ₂ +O _i	1.19	1.2 ^c , 0.8 ^d	0.68
$VO+H_{BC}$	→	VOH	2.02		
$VO+H_2$	→	VOH+H _{BC}	-0.09		
$VO+H_2$	→	VOH ₂	2.41		
$VO+2H_{BC}$	→	VOH ₂	1.19		
$VOH+H_{BC}$	→	VOH ₂	2.51		
$VOH+H_2$	→	VOH ₂ +H _{BC}	0.40		

^aThis work.^bReference 37.^cUsing MP-2³ for BZ sampling.^dUsing Γ point for BZ sampling.

The VO complex in Si has two fundamental local modes and a combination band whose frequency is estimated from a simple sum of the two fundamental A_1 and B_1 modes. The calculated values are within 10 cm⁻¹ for Si and about 20 cm⁻¹ for Ge. In Si all three modes are strongly dependent on the charge state of the complex and increase in frequency for the negative charge state. In Ge only one localized mode is found. It should be noted that within the local-density approximation (LDA), Ge is predicted to be a semimetal—the conduction-band minimum at L has the same energy as the valance-band maximum at Γ . This implies that the acceptor wave function in VO⁽⁻⁾ is delocalized and conse-

quently the calculated shift in the B_1 mode probably underestimates the true shift.

Two other configurations for the VO complex were investigated: firstly when the O atom is situated at the T lattice site, and secondly when it lies along one of the $[111]$ directions with C_{3v} symmetry. In the neutral charge state, these configurations are less stable than the C_{2v} form being 0.51 (0.10) eV and 0.26 (0.05) eV higher in Si (Ge), respectively. In the negative charge state these energies increase by factors of about 2 in Si and 4 in Ge. These results give an estimate of the activation barrier for the reorientation of the stable C_{2v} defect when its alignment changes from one $[100]$ axis

TABLE XIII. LVM's and their downward isotopic shifts (cm⁻¹) for VO and VO₂ complexes in Si and Ge. These are compared with experimental infrared data.

	Mode	Obs.	¹⁶ O			Obs.	¹⁸ O			¹⁶ O, ¹⁸ O			
			Calc. ^a	Calc. ^b	Calc. ^c		Calc. ^a	Calc. ^b	Calc. ^c	Obs.	Calc. ^a	Calc. ^b	Calc. ^c
Si: VO ⁽⁰⁾	A_1+B_1	1370.0	1387			37.5	38						
	B_1	835.8	839	843	787	35.9	37	37	38				
	A_1	~534	548	540		~1	1	3					
Si: VO ⁽⁻⁾	A_1+B_1	1430.1	1404			39.1	39						
	B_1	885.2	872	850		38.2	38						
	A_1	~545	532	539		~1	1						
Si: VO ₂	E	894	893	912	806	39	41	41	39	0, 39	0, 41	0, 41	0, 39
	A_1		593	594	656		6	7	19		3		9
	B_2		557	554	564		0	3	9		0		5
Ge: VO ⁽⁰⁾	B_1	620	642			31	33						
Ge: VO ⁽⁻⁾	B_1		643				33						
	E		690				36				0, 36		
Ge: VO ₂	A_1		363				13				6		

^aThis work.^bReference 37.^cReference 62.

into another. Electron paramagnetic (EPR) studies in Si reveal that the reorientation barrier of the neutral defect is activated with an energy of 0.38 eV in good agreement with the calculated value of 0.26 eV.^{52,53} Our calculations predict that in the negative charge state the reorientation barrier will be higher. This is in support of measurements on the recovery of the stress-induced dichroism of the 885-cm⁻¹ vibrational band, where a value between 0.4 and 0.5 eV was estimated.⁶⁷

The calculated values of the stress tensor for the VO defect in Si also depends on the charge state. For the neutral defect, we find the three principal values and directions to be $B_1 = -9.79$ eV (along [100]: the C_2 axis), $B_2 = 5.49$ eV (along [011]), and $B_3 = 4.48$ eV (along [01 $\bar{1}$]). The [011] and [01 $\bar{1}$] directions are parallel to the Si-O-Si and reconstructed Si-Si bonds, respectively. The experimental values for B_1, B_2 , and B_3 are $-11.1, 6.1$, and 4.9 eV, respectively.

For the negative charge state, B_1, B_2 , and B_3 are found to be $-6.83, 7.81$, and -0.55 eV compared with experimental values of $-8.4, 8.8$, and -0.4 eV, respectively. The change of sign of B_3 indicates that the defect is now less tensile along the "reconstructed" bond. This arises as the additional electron occupies an antibonding orbital and pushes outward the surrounding lattice. However, this argument ignores the differences in the volumes of the neutral and charged defects. In fact we found that the neutral defect led to a decrease in the volume of the supercell compared with bulk Si whereas the charged defect led to a slight increase.

VII. THE SUBSTITUTIONAL OXYGEN DIMER: VO₂

The A center in Si is known to anneal out around 300 °C with a simultaneous appearance of a strong line at 894 cm⁻¹. This line was originally assigned to the VO₂ center,⁶³ formed when an interstitial oxygen atom traps a mobile VO center. However, there are some difficulties with this assignment. The concentration of O_i appears to remain constant during the formation of the 894-cm⁻¹ band, stress splitting measurements indicate a defect with low symmetry²⁶ and, in addition, the two O atoms must be dynamically decoupled as additional modes are not detected in isotopically mixed samples.^{64,65} Previous modeling, however, supports the assignment to VO₂ with D_{2d} symmetry.^{66,57,37} There the O atoms were found to be dynamically decoupled and the calculated modes were in fair agreement with the data. In addition, when the defect anneals out three high-frequency O-related LVM's are observed which are consistent with the formation of VO₃.⁵⁷ Moreover, recent stress alignment experiments find the symmetry of the center to be D_{2d} consistent with a VO₂ defect.⁶⁷

Our results support previous theoretical work in finding the ground-state structure possesses D_{2d} symmetry. Here both oxygen atoms occupy equivalent positions by bridging atoms neighboring the vacancy as shown in Fig. 8. Structural details are given in Table XI, where it is noted that the Si-O bond lengths are shorter than in VO and there is a larger displacement of both oxygen atoms from the center of the vacancy.

Table V shows that the formation energy of the defect in Si (Ge) is 0.85 eV (1.18 eV) higher than that of the staggered dimer. Thus arguments based on simple volumetric consid-

erations implying that the aggregation of pairs of oxygen atoms lead to the creation of Si (Ge) interstitials are unlikely to be correct. The binding energy of O_i with a preexisting VO defect is 1.73 eV.

The LVM's of the defect are given in Table XIII. These are in excellent agreement with the observed 894-cm⁻¹ band and the O atoms are found to be decoupled without any additional modes appearing in the mixed isotopic case. This is in agreement with experiment.⁶⁴ The stress tensor is axial with $B_3 = -11.81$ eV and the principal direction is along the C_2 axis joining the two O atoms and $B_1 = B_2 = 5.9$ eV. It has not yet been measured.

The VO₂ center in Ge has similar properties to the Si center but has not yet been detected. The vibrational modes, given in Table XIII, consist of modes at 690 and 363 cm⁻¹.

VIII. INTERACTION OF VO WITH HYDROGEN

It is known that hydrogen complexes with single vacancies by saturating the Si or Ge dangling bonds lead to VH_n defects where n runs from 1 to 4.⁶⁸⁻⁷¹ In addition, recent work has demonstrated that hydrogen is easily trapped by the A center in Si-forming VOH_n defects where n is 1 or 2. The latter produces infrared-absorption bands at 2151, 2126, and 943 cm⁻¹, which were assigned to the symmetric and asymmetric stretch modes of Si-H and the asymmetric stretch mode of the oxygen atom, respectively.⁷² However, no indication of the presence of the partially passivated A center (VOH) was found in this work.

The VOH center was suggested to account for the E3 deep-level transient spectroscopy acceptor level at $E_c - 0.31$ eV formed in proton-implanted floating-zone Si crystals.⁷³ EPR experiments identify the center which persists until 290 °C in proton-implanted CZ Si.⁷⁴ The hyperfine interaction with the proton located 2.5 Å from the Si atom with a dangling bond was resolved. The defect has C_{1h} symmetry below 180 K, but above 240 K the center possesses C_{2v} symmetry arising from a thermally activated hopping of the H atom between dangling bonds.^{74,75} The activation energy for the hopping of H and D atoms was found to be 0.18 and 0.26 eV, respectively, for the neutral defect. The same C_{2v} symmetry was found from a recent stress Laplace DLTS study on the E3 center.⁷⁵ This is because the electron emission rate measured in DLTS occurred at a temperature where the H atom was able to hop between Si dangling bonds.

No vibrational modes of the defect have been reported to date. Previously, the defect had been investigated theoretically using a Hartree-Fock cluster method.⁷⁶

A. Theoretical results

Relaxation of the neutral VOH defect with C_{1h} symmetry gave the Si-H and Si-O lengths to be 1.50 and 1.68 Å. The distance between the H atoms and the Si atoms with a dangling bond is 2.7 Å in good agreement with the experimental estimate of 2.5 Å. The vibrational modes are given in Table XIV. The vibrational activity of VOH arises from almost decoupled oscillations of Si-O-Si and Si-H units. The 854-cm⁻¹ mode is due to an asymmetric stretch of Si-O-Si while hydrogen-related stretch and bend modes are found at 2042, 578, and 532 cm⁻¹, respectively. These are recog-

TABLE XIV. LVM's of VOH in Si and their downward isotopic shifts (cm^{-1}) for ^{18}O and D substitution. *R* labels indicate resonant modes.

	^{16}O , H	^{18}O , H	^{16}O , D	^{18}O , D
VOH ⁽⁰⁾	2042.4	0.0	575.3	575.4
	854.4	37.6	0.0	37.6
	578.5	0.0	R	R
	565.2	1.5	5.9	7.8
	532.5	0.4	R	R
VOH ⁽⁻⁾	2045.7	0.0	576.0	576.0
	901.2	40.2	0.0	40.0
	594.3	0.0	R	R
	571.8	0.3	5.5	6.9
	554.1	1.6	R	R

nized as such from the displacements of these atoms in the modes. Mixed isotopic data show these modes are almost decoupled. The 565-cm^{-1} mode is a breathing mode showing a small shift for both ^{18}O and D substitution. The Si-D wag modes fall within the lattice modes, and thus no isotopic shifts are available in Table XIV. In the negative charge state, the 854-cm^{-1} mode increases to 901 cm^{-1} . This mirrors the changes in the local mode of VO when it traps an electron.

The activation energy for H hopping between the Si dangling bonds can be found by relaxing the defect with C_{2v} symmetry. This gave a barrier E_a of 0.11 eV for the neutral defect but this neglects the zero-point energy of the H atom. If we assume that the contribution of this vanishes at the saddle point, where the Si-H bonds are very long at 1.80 \AA , then the barrier will include the contribution of $-\hbar\omega/2$ where ω is the frequency of the Si-H stretch mode given in Table XIV. The inclusion of this term effectively eliminates the barrier and implies that tunneling must become important. It is known that the barrier is apparently greater in the D case by about 0.07 eV.⁷⁴ For the negatively charged center, the barrier increases to 0.18 eV.

In addition to the hopping of H, the O atom can also jump between different $\langle 100 \rangle$ axes. An upper limit to this barrier can be found by constraining both O and H to lie on the same $\langle 111 \rangle$ axis. E_a for this configuration is 0.42 and 0.72 eV for the neutral and negatively charged defects, respectively. These values are greater than found for the A-center consistent with the view that both H and a trapped electron impede the hopping of the O atom.

Table XII shows that a hydrogen molecule is not stable when VO centers are present, and will dissociate to form VOH₂ defects. This explains the lack of observations of VOH in samples into which molecular hydrogen is diffused.⁷² Nevertheless, there is a binding energy of 2 eV between the A center and an isolated bond-centered H atom suggesting that VOH centers, once formed, can be stable to temperatures around 300°C .

IX. CONCLUSIONS

The *ab initio* calculations carried out using Gaussian orbitals in large supercells have revealed a number of features not found previously. In Si, the effect of pressure on the local modes of interstitial oxygen is entirely consistent with the view that, at low pressures, the defect has D_{3d} symmetry with an effective Si-O-Si angle of 180° . However, the barrier to a bent Si-O-Si configuration increases with increasing pressure so that the defect eventually assumes a buckled form. Nevertheless, the oxygen atom can still rotate around the $\langle 111 \rangle$ axis. This is the stable form for the defect in Ge. The oxygen interstitial in Si possesses three high-frequency fundamental modes. Besides the well-known asymmetric stretch mode at 1136 cm^{-1} , there is an infrared inactive A_{1g} mode around 621 cm^{-1} and an E_u mode localized on the Si neighbors to the oxygen atom lying just below the Raman edge. The diffusion of O_i has been considered and the calculated activation barrier is about 2.2 eV in Si and 1.7 eV in Ge which are within 0.3 eV of the experimental values.

The piezospectroscopic tensors for the local modes as well as the stress tensor for the defect have been evaluated here. The stress tensor demonstrates that the reconstructed bond in VO breaks when an electron occupies the antibonding state and the atoms with broken bonds move away from each other compressing the lattice. This type of calculation can be extended to many defects and links directly total-energy calculations with spectroscopic data obtained from stressed crystals in which defects have been aligned.

The oxygen dimer, in both Si and Ge, is stable in the staggered form with modes calculated to be in good agreement with experiment. It is surprising that the two stretch modes of the dimer, in which the oxygen atoms share a common Si neighbor, are ‘‘almost’’ dynamically decoupled. The anomalous temperature dependence for the modes in Si has been linked to an increased buckling occurring during the contraction of the crystal when cooled. This seems to be a signature of a buckled oxygen bridge in Si and its observation has implications for other defects. The dimer is found to be stable against the formation of O_2 molecules and VO_2 defects. The barrier to diffusion of the dimer is about 0.8 eV and 0.6 eV lower in Si and Ge, respectively, than that of O_i . The diffusion path involves a concerted movement of the pair of atoms along a path which eliminates dangling bonds at the saddle point.

The VO and VO_2 defects are examined and it is found that charging the former defect leads to an increase in frequency as observed, while the latter is responsible for the 894-cm^{-1} band in Si. Confirmation that the 894-cm^{-1} band is due to VO_2 could come from an evaluation of the stress tensor which is given here. The VOH defect is remarkable in that the H and O atoms can break their bonds leading to reorientation of the defect with activation barriers of a few tenths of an eV. The barriers are larger for the negatively charged defects.

ACKNOWLEDGMENTS

We thank TFR in Sweden for financial support. We also acknowledge support from INTAS under Grant No. 97-0824.

- ¹*Oxygen in Silicon*, edited by F. Shimura, Semiconductors and Semimetals Vol. 42 (Academic Press, Orlando, 1994).
- ²*Early Stages of Oxygen Precipitation in Silicon*, edited by R. Jones, NATO Advance Science Institutes, Series 3: High Technology, Vol. 17 (Kluwer Academic, Dordrecht, 1996).
- ³R.C. Newman, *J. Phys.: Condens. Matter* **12**, R335 (2000).
- ⁴C.S. Fuller, J.A. Ditzenberger, N.B. Hannay, and E. Buchler, *Phys. Rev.* **96**, 833 (1954).
- ⁵M.D. McCluskey and E.E. Haller, *Phys. Rev. B* **56**, 9520 (1997).
- ⁶G. D. Watkins, in *Early Stage of Oxygen Precipitation in Silicon*, Ref. 2, p. 1.
- ⁷J.C. Mikkelsen, in *Oxygen, Carbon, Hydrogen, and Nitrogen in Crystalline Silicon*, edited by B. C. Giessen, D. E. Polk, and A. I. Taub, Mater. Res. Soc. Symp. Proc. No. **59** (MRS, Pittsburgh, 1986), p. 19.
- ⁸M. Ramamoorthy and S.T. Pantelides, *Phys. Rev. Lett.* **76**, 267 (1996).
- ⁹M. Needels, J.D. Joannopoulos, Y. Bar-Yam, and S.T. Pantelides, *Phys. Rev. B* **43**, 4208 (1991).
- ¹⁰A. Oshiyama and M. Saito, *Defect Control in Semiconductors*, edited by K. Sumino (Elsevier Science Publishers, New York, 1990).
- ¹¹H.B. Capaz, L.V.C. Assali, L.C. Kimerling, K. Cho, and J.D. Joannopoulos, *Phys. Rev. B* **59**, 4898 (1999).
- ¹²M. Needels, J.D. Joannopoulos, Y. Bar-Yam, S.T. Pantelides, and R.H. Wolfe, in *Defects in Materials*, edited by P.D. Bristowe, J.E. Epperson, J.E. Griffith, and Z. Liliental-Weber, Mater. Res. Soc. Symp. Proc. No. **209** (MRS, Pittsburgh, 1991), p. 103.
- ¹³C.P. Flynn, *Phys. Rev. Lett.* **35**, 1721 (1975).
- ¹⁴L.I. Murin, T. Hallberg, V.P. Markevich, and J.L. Lindström, *Phys. Rev. Lett.* **80**, 93 (1998).
- ¹⁵S. Öberg, C.P. Ewels, R. Jones, T. Hallberg, J.L. Lindström, L.I. Murin, and P.R. Briddon, *Phys. Rev. Lett.* **81**, 2930 (1998).
- ¹⁶M. Pesola, J. von Boehm, and R.M. Nieminen, *Phys. Rev. Lett.* **82**, 4022 (1999).
- ¹⁷C.P. Ewels, Ph.D. thesis, University of Exeter, 1997.
- ¹⁸M. Ramamoorthy and S.T. Pantelides, *Solid State Commun.* **106**, 243 (1998).
- ¹⁹J.P. Perdew and Y. Wang, *Phys. Rev. B* **45**, 13 244 (1992).
- ²⁰G.B. Bachelet, D.R. Hamann, and M. Schlüter, *Phys. Rev. B* **26**, 4199 (1982).
- ²¹H.J. Monkhorst and J.D. Pack, *Phys. Rev. B* **13**, 5188 (1976).
- ²²R. Jones and P.R. Briddon, in *Identification of Defects in Semiconductors*, edited by M. Stavola, Semiconductors and Semimetals, Vol. 51A (Academic Press, San Diego, 1998).
- ²³F. Birch, *J. Geophys. Res.* **57**, 227 (1952).
- ²⁴R. Jones, S. Öberg, and A. Umerski, *Mater. Sci. Forum* **83-87**, 551 (1991).
- ²⁵R.C. Newman and R. Jones, in *Oxygen in Silicon*, Ref. 1, p. 289.
- ²⁶D.R. Bosomworth, W. Hayes, A.R.L. Spray, and G.D. Watkins, *Proc. R. Soc. London, Ser. A* **317**, 133 (1970).
- ²⁷H. Yamada-Kaneta, C. Kaneta, and T. Ogawa, *Phys. Rev. B* **42**, 9650 (1990).
- ²⁸H. Yamada-Kaneta, *Phys. Rev. B* **58**, 7002 (1998).
- ²⁹T. Hallberg, L.I. Murin, J.L. Lindström, and V.P. Markevich, *J. Appl. Phys.* **84**, 2466 (1998).
- ³⁰M. Gienger, M. Glaser, and K. Laßmann, *Solid State Commun.* **86**, 285 (1993).
- ³¹W. Kaiser, *J. Phys. Chem. Solids* **23**, 255 (1962).
- ³²R. Jones, A. Umerski, and S. Öberg, *Phys. Rev. B* **45**, 11 321 (1992).
- ³³L.C. Snyder, R. Wu, and P. Deák, *Radiat. Eff. Defects Solids* **111&112**, 393 (1989).
- ³⁴E. Artacho, F. Ynduráin, B. Pajot, R. Ramirez, C.P. Herrero, L.I. Khirunen, K.M. Itoh, and E.E. Haller, *Phys. Rev. B* **56**, 3820 (1997).
- ³⁵D. Shaw, in *Atomic Diffusion in Semiconductors* (Plenum, New York, 1973).
- ³⁶M. Imai, H. Noda, M. Shibata, and Y. Yatsurugi, *Appl. Phys. Lett.* **50**, 395 (1987).
- ³⁷M. Pesola, J. von Boehm, T. Mattila, and R.M. Nieminen, *Phys. Rev. B* **60**, 11 449 (1999).
- ³⁸B. Pajot, E. Artacho, C.A.J. Ammerlaan, and J-M. Spaeth, *J. Phys.: Condens. Matter* **7**, 7077 (1995).
- ³⁹A.J. Mayur, M.D. Sciacca, M.K. Udo, A.K. Ramdas, K. Itoh, J. Wolk, and E.E. Haller, *Phys. Rev. B* **49**, 16 293 (1994).
- ⁴⁰H.J. Hrostowski and R.H. Kaiser, *Phys. Rev. B* **107**, 966 (1957).
- ⁴¹M. D. McCluskey (private communication).
- ⁴²E. Martínez, J. Plans, and Felix Ynduráin, *Phys. Rev. B* **36**, 8043 (1987).
- ⁴³K. Laßmann, C. Linsenmaier, F. Maier, F. Zeller, E.E. Haller, K.M. Itoh, L.I. Khirunen, B. Pajot, and H. Müssig, *Physica B* **263-264**, 384 (1999).
- ⁴⁴J.W. Corbett, R.S. McDonald, and G.D. Watkins, *J. Phys. Chem. Solids* **25**, 873 (1964).
- ⁴⁵P. Wagner, J. Hage, J.M. Trombetta, and G.D. Watkins, *Mater. Sci. Forum* **83-87**, 401 (1992).
- ⁴⁶D. Åberg, B.G. Svensson, T. Hallberg, and J.L. Lindström, *Phys. Rev. B* **58**, 12 944 (1998).
- ⁴⁷S.A. McQuaid, B.K. Johnson, D. Gambaro, R. Falster, M.J. Ashwin, and J.H. Tucker, *J. Appl. Phys.* **86**, 1878 (1999).
- ⁴⁸U. Gösele and T.Y. Tan, *Appl. Phys. A: Solids Surf.* **28**, 79 (1982).
- ⁴⁹D.J. Chadi, *Phys. Rev. Lett.* **77**, 861 (1996).
- ⁵⁰R.E. Whan, *Phys. Rev.* **140**, A690 (1965).
- ⁵¹A.A. Klechko, V.V. Litvinov, V.P. Markevich, and L.I. Murin, *Fiz. Tekh. Poluprovodn.* **33**, 1287 (1999) [*Semiconductors* **33**, 1163 (1999)].
- ⁵²G.D. Watkins and J.W. Corbett, *Phys. Rev.* **121**, 1001 (1961).
- ⁵³G.D. Watkins and J.W. Corbett, *Phys. Rev.* **121**, 1015 (1961).
- ⁵⁴N. Fukuoka, H. Saito, and Y. Kambe, *Jpn. J. Appl. Phys., Part 1* **22**, L353 (1983).
- ⁵⁵A. Resende, R. Jones, S. Öberg, and P.R. Briddon, *Phys. Rev. Lett.* **82**, 2111 (1999).
- ⁵⁶A.R. Bean and R.C. Newman, *Solid State Commun.* **9**, 271 (1971).
- ⁵⁷C.P. Ewels, R. Jones, and S. Öberg, *Mater. Sci. Forum* **196-201**, 1297 (1995).
- ⁵⁸L.I. Murin, V.P. Markevich, T. Hallberg, and J.L. Lindström, *Solid State Phenom.* **69-70**, 309 (1999).
- ⁵⁹J.L. Lindström, L.I. Murin, V.P. Markevich, T. Hallberg, and B.G. Svensson, *Physica B* **273-274**, 291 (1999).
- ⁶⁰M.J. Puska, S. Pöykkö, M. Pesola, and R.M. Nieminen, *Phys. Rev. B* **58**, 1318 (1998).
- ⁶¹A. Fazzio, A. Janotti, and A.J.R. da Silva, *Phys. Rev. B* **61**, R2401 (2000).
- ⁶²B. Pajot, S. McQuaid, R.C. Newman, C. Song, and R. Rahbi, *Mater. Sci. Forum* **143-147**, 969 (1994).
- ⁶³J.W. Corbett, G.D. Watkins, and R.S. McDonald, *Phys. Rev.* **135**, A1381 (1964).
- ⁶⁴F.A. Abou-el-Fotouh and R.C. Newman, *Solid State Commun.* **15**, 1409 (1974).

- ⁶⁵B.J. Svensson and J.L. Lindström, Phys. Rev. B **34**, 8709 (1986).
- ⁶⁶G.G. Deleo, C.S. Milsted, and J.C. Kralik, Phys. Rev. B **31**, 3588 (1985).
- ⁶⁷B. Bech Nielsen (unpublished).
- ⁶⁸B. Bech Nielsen, L. Hoffmann, M. Budde, R. Jones, J. Goss, and S. Öberg, Mater. Sci. Forum **196-201**, 933 (1995).
- ⁶⁹B. Bech Nielsen, P. Johannesen, P. Stallinga, K. Bonde Nielsen, and J.R. Byberg, Phys. Rev. Lett. **79**, 1507 (1997).
- ⁷⁰S.K. Estreicher, Mater. Sci. Eng., R. **14**, 319 (1995).
- ⁷¹B.J. Coomer, P. Leary, M. Budde, B. Bech Nielsen, R. Jones, S. Öberg, and P.R. Briddon, Mater. Sci. Eng., B **58**, 36 (1999).
- ⁷²V.P. Markevich, L.I. Murin, M. Suezawa, J.L. Lindstrom, J. Coutinho, R. Jones, P.R. Briddon, and S. Öberg, Phys. Rev. B **61**, 12 964 (2000).
- ⁷³B.G. Svensson, A. Hallen, and B.U.R. Sundqvist, Mater. Sci. Eng., B **4**, 285 (1989).
- ⁷⁴P. Johannesen, B. Bech Nielsen, and J.R. Byberg, Phys. Rev. B **61**, 4659 (2000).
- ⁷⁵K. Bonde Nielsen, L. Dobaczewski, K. Goscinski, R. Bendesen, Ole Andersen, and B. Bech Nielsen, Physica B **273-274**, 167 (1999).
- ⁷⁶E. Artacho and F. Ynduráin, Solid State Commun. **72**, 393 (1989).
- ⁷⁷P. J. Mohr and B. N. Taylor, Rev. Mod. Phys. **72**, 351 (2000).
- ⁷⁸Jasprit Singh, *Physics of Semiconductors and Their Heterostructures* (McGraw-Hill, New York, 1993).